Enhanced Performance of Charging Stations via Converter Control Under Unbalanced and Harmonic Distorted Grids

Hoach The Nguyen, *Member, IEEE*, Ameena Saad Al Sumaiti, *Senior Member, IEEE*, Khalifa Al Hosani, *Senior Member, IEEE*, Khaled Al Jaafari, *Member, IEEE*, Young-Ji Byon, *Member, IEEE*, Jamal Yousuf Alsawalhi, *Member, IEEE*, and Mohamed Shawky El Moursi, *Senior Member, IEEE*

***Abstract*—This article proposes a new control structure for grid-interfaced converters to enhance ancillary services from emerging electric vehicle (EV) charging stations (CS) under unbalanced and distorted grid conditions. Compared to existing methods, the proposed control structure is relatively simple yet effective for both regulating powers and minimizing harmonics under unbalanced and distorted grid conditions. A simple direct predictive control methodology is proposed where the positive fundamental component of currents is controlled for power regulation while other negative sequence or harmonic current components are set to zeros. Consequently, the charging station operation is enhanced with efficient ancillary services to the electric grid. The novelty originates from a simple predictive control structure in an *abc*-natural frame without adding any decoupled or separated current-component controllers. Comparative studies on both Matlab/Simulink platform and OPAL-RT-based real-time system among proportional integral (PI) control, finite predictive control, and the proposed method are conducted to verify the efficacy of the proposed structure. The comparative results show that the control structure improves the control performance and significantly enhances the support for the local loads under unbalanced, harmonic distorted grid conditions.**

***Index Terms*—Grid-interfaced converter, EV charging station, deadbeat control, direct predictive control, harmonics, unbalanced and distorted grid.**

Manuscript received August 7, 2020; revised November 28, 2020; accepted January 11, 2021. Date of publication January 18, 2021; date of current version November 22, 2021. This work was supported by Khalifa University, Abu Dhabi, United Arab Emirates under Award No. KKJRC-2019-Trans2. Paper no. TPWRD-01215-2020. *(Corresponding author: Mohamed Shawky El Moursi.)*

Hoach The Nguyen is with the Electrical Engineering and Computer Science (EECS) Department, Khalifa University, Abu Dhabi 127788, UAE, on leave from the Department of Energy, Hanoi Architectural University, Hanoi, Vietnam (e-mail: nthoach@gmail.com).

Ameena Saad Al Sumaiti, Khalifa Al Hosani, Khaled Al Jaafari, and Jamal Yousuf Alsawalhi are with the Advanced Power and Energy Center (APEC), EECS Department, Khalifa University, Abu Dhabi 127788, UAE (e-mail: ameena.alsumaiti@ku.ac.ae; khalifa.halhosani@ku.ac.ae; khaled.aljaafari@ku.ac.ae; jamal.alsawalhi@ku.ac.ae).

Young-Ji Byon is with the Department of Civil Infrastructure and Environmental Engineering, Khalifa University, Abu Dhabi 127788, UAE (e-mail: youngji.byon@ku.ac.ae).

Mohamed Shawky El Moursi was with the Advanced Power and Energy Center (APEC), Department of Electrical Engineering and Computer Science, Khalifa University, Abu Dhabi 127788, United Arab Emirates, on leave from the Faculty of Engineering, Mansoura University, Mansoura 35516, Egypt (e-mail: mohamed.elmoursi@ku.ac.ae).

Color versions of one or more figures in this article are available at https://doi.org/10.1109/TPWRD.2021.3052319.

Digital Object Identifier 10.1109/TPWRD.2021.3052319

NOMENCLATURE

Abbreviations

APF	Active Power Filter
BESS	Battery Energy Storage System
CS	Charging Station
EV	Electric Vehicle
FCS	Finite Control Set
GCC	Grid-Connected Converter
MPC	Model Predictive Control
MMC	Modular Multilevel Converter
NPC	Neutral-Point-Clamped (converter)
PCC	Point of Common Coupling
PI	Proportional-Integral
PRO	Proposed Control Structure
PWM	Pulse Width Modulation
RES	Renewable Energy Source
V1G	Unidirectional managed charging services
V2G	Vehicle-to-Grid
V2H/B	Vehicle-to-Home/-Building

Variables

u_{dq}	Grid voltages in *dq*-frame
i_{dq}	GCC currents in *dq*-frame
u_x	Phase voltages of grid, $x = \{a, b, c\}$
i_x, i_{Lx}, i_{gx},	Phase currents of GCC, local loads, total current injected into grid, respectively
vx	Terminal phase-voltages of GCC
s_x	Switching state of leg x, $s_x \in \{0, 1\}$
v_{dc}, i_{dc}, i_L	*dc*-voltage, total *dc*-current, dc-load current, respectively
s, p, q	Instantaneous Apparent-, Real-, Imaginary-Power, respectively
P, Q	Active-, Reactive-Power, respectively

Subscripts and Superscripts

x	$x = \{a, b, c\}$, $\{\alpha, \beta\}$, or $\{d, q\}$ up to the reference frame
$\overline{X}$	Slow-dynamic component of variable X
X_{ref}, X^{ref}	Reference value of variable X
$X^{(+1)}$	Positive sequence fundamental component of X
$X^{(n)}$	The n^{th} harmonic component of X
X^{db}	Deadbeat unconstrained value of control input X

I. Introduction

RECENTLY, charging stations have become an essential component of modern urban infrastructure for electrified transportation systems as the global energy crisis and environmental issues urge for a green transportation paradigm with electric vehicles (EV) [1]–[3]. More charging stations have been newly connected to distribution networks [4]. Typical smart-charging approaches for a charging station include unidirectional controlled charging (V1G), bidirectional vehicle-to-grid (V2G), and vehicle-to-home/-building (V2H/B) [5]. That is, EVs can provide a range of services for the power system since they are parked most of the time (i.e., 90–95%) [6]. An effective interoperation between aggregated fleets of EVs and the grid can be realized by an aggregated interface between charging stations and the grid [7], [8]. In this context, grid-interfaced converters of the charging stations accompanied by control structures play a central role for grid-to-vehicles, vehicle-to-grid operations, and renewable energy integration in smart-grids [3], [4], [9]. Smart charging stations are a typical example of the interoperation among smart-grid and fleets of electric vehicles [10]. Therefore, charging stations can actively participate in power-quality improvement of distribution grids.

The power-quality in distribution grids can be deteriorated under various critical conditions. For example, power electronic devices such as uncontrolled rectifiers generate significant harmonic distortions into the grid [9], [11], [12]. Also, different batteries and charging technologies employed in a smart charging station with sophisticated EV charging algorithms, can cause distorted currents spreading in the network [13], [14]. Highly uncertain harmonics injected to the grid may cause voltage harmonics and serious problems of power transfer in power networks [11], [12], [15]. Hence, additional hardware costs on active power filters (APF) may incur to compensate for the uncertain load current harmonics and unbalanced networks. Furthermore, the requirements of fault ride-through in emerging smart-grids force the smart charging stations to work under critical grid conditions including unbalanced and harmonic distorted voltages [16]–[18]. Consequently, conventional control methods may exhibit highly distorted grid currents and *dc*-voltage ripples degrading the power-quality on both the grid and load sides [19].

A variety of control structures have been applied to grid-connected converters (GCC) in the existing literature. Current challenges on the GCC control are mainly on control performances under critical grid conditions and potentially supporting the distribution grid [17], [18]. That is, the authors in [14] concluded that a controlled EV charging system can significantly reduce unbalances in networks, especially for long distribution feeders. A number of works on grid-connected converter control [20]–[28] have been published focusing on improving the grid-injected currents of active front-end rectifiers. Meanwhile, the GCCs are used to improve the power-quality at the point of common coupling (PCC) of a 3-phase 4-wire system in [15] with functions of an active power filter in addition to the real power generation from renewable energy sources (RES) to the grid. The presented scheme in [15] considered the support to local load distorted currents while it did not consider the unbalanced or distorted grid conditions. Another research work in [29] developed a dynamic model and control schemes considering both positive- and negative-sequences to deal with unbalanced grid conditions, but not for harmonic distortion in general. Similarly, the unbalanced grid condition is also taken into account in [30]–[35] as a challenge under different control strategies. The unbalance component which is a symmetrical negative sequence of fundamental frequency can be treated in the same way with general harmonic components in the control algorithm. Hence, there is a need for research and investigation on general undesired sequences and harmonic distortion.

To tackle the challenges under critical grid conditions, recent research works focus on both unbalanced and distorted grid conditions. Unfortunately, the general harmonic components are unpredictable with different frequencies depending on a variety of generating sources. Therefore, there are challenges for passive filer design as well as control design of active filters to eliminate these undesired harmonics. There is a great chance to deal with harmonic generation at a distribution level via controlling the grid-interfaced converters. However, there are few published works on the GCC control under both unbalanced and general distorted conditions. For example, Zhang *et al.* in [36] recently suggested a predictive control method for the PWM rectifier which was tested for both unbalanced and distorted grid cases using the extended *p-q* theory. However, the cancellation of general harmonic distortion was not fully presented in the presented control structure [36]. The authors of [37] used repetitive current controllers to minimize the odd-order harmonics of supply currents caused by distorted and unbalanced voltage conditions. The control system in [37] is complicated due to decoupled controllers in *dq*-frame, positive and negative sequence controllers, and repetitive control components. To the best of our knowledge, there are no simple control structure, which can simultaneously deal with unbalanced, general distorted voltages in addition to the grid-support functions.

Therefore, a new control structure is proposed in this paper to enhance the grid support by utilizing emerging electric vehicle (EV) charging stations (CS) under unbalanced, and harmonic distorted grid conditions. Especially, a special mode is proposed to support critical local loads by compensating for reactive power, unbalanced and distorted currents injected into the grid. The new control structure offers the following advantages compared to other control schemes in the literature:

- All the controllers are designed and implemented in an *abc*-natural frame to avoid intermediate transformation for simplicity.
- The sequence harmonic component extraction is only required for the fundamental positive grid voltage.
- Only one composite current controller for two-phases is used.
- The proposed direct selection of switching states without exhaustive search based on simple predictive deadbeat inputs avoids computational burdens from the conventional exhaustive search.
- The switching frequency is minimized without forfeiting control performances using a very simple approach by selecting zero switching-states.

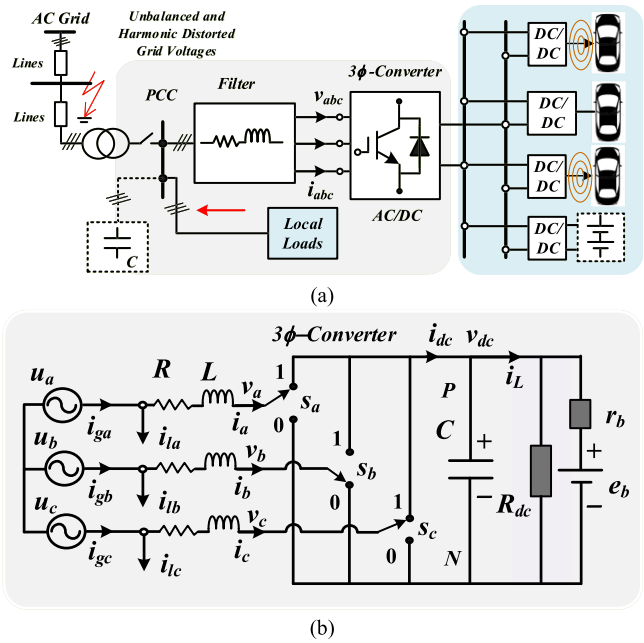

Fig. 1. Charging station for electric vehicles interacting with distribution grid. (a) Overall diagram of a smart charging station providing *DC* fast charging points under highly distorted currents from local loads connected to the grid and critical conditions of the grid. (b) Equivalent circuit of the system with interfacing converter model.

- The proposed single control structure can manage multiple control tasks including regulating fundamental current components and cancelling out other unexpected components.
- A special working mode is proposed to compensate for reactive power, unbalanced and distorted currents from local load currents.

Comparative studies are conducted on both Matlab/Simulink platform and real-time digital simulator (OPAL RT-5700) among proportional integral (*PI*), finite predictive control (*FCS-MPC*), and the proposed method structures (*PRO*). The efficacy of the proposed structure is verified in unbalanced, harmonic distorted grid conditions, and nonlinear local loads.

This paper is organized into five sections. Section II presents the theory of instantaneous powers in case of general harmonic voltages and currents. Then, the control objectives of charging stations via interface converters are determined by reference-current settings. Section III proposes an innovative current control structure to realize the objectives. Comparative studies and performance verification are presented in Section IV. Section V offers conclusion and promising future applications of the proposed control structure.

II. Instantaneous Powers and Reference Current Settings

This section introduces the power transfer between EV charging stations and power grid using the *pq*-theory to formulate the control problem. Fig. 1 illustrates a typical EV charging station connected to a distribution grid with local loads. In Fig. 1(a), EVs are charged via offboard *DC*-fast charging posts or wireless charging pads where the battery storage may be facilitated in the charging station. A three-phase converter with a capability of bidirectional power transfer is used to interface with the power grid. An *RL* filter is used between the GCC and the PCC where local loads are also connected. Fig. 1(b) shows the equivalent circuit of the converting system with converter model and grid voltage at PCC. In this circuit model, the chargers are generally modeled as dc-loads and dc-sources with a battery model due to the bidirectional power flow capability. The charging station supports EVs' chargers by maintaining the constant dc-bus voltage in form of a constant-voltage source and each charger has specific charging algorithms under its own control system. Meanwhile, this paper focuses on the grid-interfaced converter under critical grid-conditions and the proposed functionalities to support the grid.

The two-level (2L) VSC is the most widely-used topology for charging stations due to the recent development of power switches with higher power ratings and switching frequency. Furthermore, the rating power of the charging station with 2-VSC can be efficiently utilized for dc-fast charging ports using the switch-port mechanism. That is, multiple normal charging ports can be switched into a few dc-fast charging ports when necessary. In high-power applications, different topologies such as multilevel converters (i.e., neutral point clamped – NPC or modular multilevel converters-MMC) can be used.

The *pq*-theory is used to identify the instantaneous real and imaginary power between the grid and charging stations in general form. First, the grid voltage and current are written in a form of harmonic components as:

$$u_{dq} = u_{dq}^{(1)} + \sum_{n\neq 1} u_{dq}^{(n)} e^{j(n-1)\omega t},$$
$$i_{dq} = i_{dq}^{(1)} + \sum_{n\neq 1} i_{dq}^{(n)} e^{j(n-1)\omega t} \quad (1)$$

where the superscript $x^{(1)}$ represents the fundamental positive sequence component, $x^{(n)}$ represents the n^{th} harmonic component in an *abc*-frame with $n > 0$ for a positive sequence and $n < 0$ for a negative sequence.

The instantaneous power is defined by a complex number as:

$$s = u_{dq} i_{dq}^{*} = p + jq \quad (2)$$

$$p = u_d^{(1)} i_d^{(1)} + u_q^{(1)} i_q^{(1)} + real\left(\sum_{(n,m)\neq(1,1)} u_{dq}^{(n)} i_{dq}^{*(m)} e^{j(n-m)\omega t}\right) \quad (3)$$

$$q = u_q^{(1)} i_d^{(1)} - u_d^{(1)} i_q^{(1)} + imag\left(\sum_{n,m\neq(1,1)} u_{dq}^{(n)} i_{dq}^{*(m)} e^{j(n-m)\omega t}\right) \quad (4)$$

where the superscript $^{(*)}$ represents the conjugate complex number, $real(*)$ and $imag(*)$ represent the real and imaginary parts of the complex number x, respectively.

The first control objective is set to cancel out all the undesired harmonic current components ($n \neq 1$) as follows:

$$i_{dq}^{(n)ref} = 0,\ \forall n \neq 1 \tag{5}$$

where the superscript (^{ref}) denotes the reference value set to the relevant current components. The settings by (5) minimize potential ripples in the instantaneous active power to reduce ripples in v_{dc}. Note that, a special case for $n = -1$ represents the unbalanced grid voltage with negative sequence as a specific case of general harmonics.

In general, the reference harmonic currents in (5) can be set to compensate for the distorted local load currents in extended applications. The compensating harmonic currents will cancel out the harmonic components from the distorted local loads injected into the grid.

Consequently, average values of instantaneous powers (p and q) depend only on the fundamental positive sequence component of voltage and current as expected. These powers are set at stable references as follows:

$$\begin{aligned} \bar{p} &= u_d^{(1)} i_d^{(1)} + u_q^{(1)} i_q^{(1)} = \bar{P}_{ref}, \\ \bar{q} &= u_q^{(1)} i_d^{(1)} - u_d^{(1)} i_q^{(1)} = \bar{Q}_{ref} \end{aligned} \tag{6}$$

Therefore, stabilizing conditions of the *dc*-link voltage depend on how to cancel out the oscillating components of the real power p shown in (3). For general harmonic distorted grid voltages, even all other harmonic currents ($n \neq 1$) are cancelled out, there are still oscillations in instant real power, p due to the interaction between $i^{(1)}{}_{dq}$ and $u^{(n)}{}_{dq}$ ($n \neq 1$). This is a trade-off in the GCC control theory as discussed in [38].

Hence, the current references are simply set for fundamental positive-sequence currents as:

$$\begin{aligned} i_d^{(1)ref} &= \frac{u_d^{(1)} \bar{P}_{ref} + u_q^{(1)} \bar{Q}_{ref}}{\left(u_d^{(1)}\right)^2 + \left(u_q^{(1)}\right)^2}, \\ i_q^{(1)ref} &= \frac{u_q^{(1)} \bar{P}_{ref} - u_d^{(1)} \bar{Q}_{ref}}{\left(u_d^{(1)}\right)^2 + \left(u_q^{(1)}\right)^2} \end{aligned} \tag{7}$$

In summary, the current control objectives set by (5) and (7) ensure harmonic cancellation and stable average power exchange via the fundamental current components only. First, the harmonic currents are cancelled out to ensure power-quality in the distribution grid. Second, the *dc*−voltage of the charging station can be regulated with minimal ripples by allowing only the fundamental currents to transfer powers. Third, by setting the $\overline{Q}_{ref}$, the charging station converter can compensate for the reactive power of local loads to improve the power factor at the PCC. In addition, the converter currents can be flexibly set to compensate the harmonic distortion of distorted local loads while accepting additional v_{dc} ripples as a proposed working mode of the charging station. In this case, the ripples can be tackled by the BESS connected at the *dc* link as shown in Fig. 1(a) if it is necessary.

III. Simple Current Control Structure Based on Robust Direct Predictive Control

This section derives a robust direct predictive control in an *abc*–reference frame with a very simple structure to realize the control objectives mentioned in Section II. The general dynamics of phase current and *dc*-link voltage are written for phase *a* and *b* based on the Kirchoff's law as follows:

$$L\frac{di_x}{dt} = -Ri_x + u_x - v_x \tag{8}$$

$$C\frac{dv_{dc}}{dt} = i_{dc} - i_L = \sum_{x=\{a,b,c\}} i_x s_x - i_L \tag{9}$$

where u_x, i_x, and $v_x \mid x = \{a, b, c\}$ denote the phase quantities of grid-voltage, grid currents, and converter's terminal voltages, respectively. v_{dc} and i_L are the *dc* link voltage and the *dc*-load current, respectively. R and L are the equivalent resistance and inductance of the *RL* filter, respectively. C is the equivalent capacitance of the *dc*-link bus and $i_{dc} = \Sigma i_x s_x$, $x = \{a, b, c\}$ following the *Kirchoff*'s law on current where s_x is the switching function representing the discrete nonlinearity of the system with $s_x = \{0, 1\}$. The discrete state, $s_x = 1$, means the upper switch/arm of leg-x is closed and vice versa. The lower switch/arm is in complementary switching-state of the upper one to avoid the short-circuit of the *dc*-voltage. The ideal switches are assumed by neglecting the commutation process in control design step. In practice, the deadtime is set for power switches to avoid short-through in switching legs which can result into negative effects on control performances with more distortion. However, the controller is designed with high-bandwidth for fast-dynamic response to compensate for the deadtime effects. All symbols are shown in Fig. 1(b) for convenience. Note that $i_c = -i_a - i_b$ due to a three-wire system.

A. Robust Prediction Model With Disturbance Observers

For a robust control system, the real values of parameters R, L, and C are assumed to be unknown where only nominal values are available from the manufacturers. Hence, the dynamic equations (8)–(9) are rewritten in general forms with additional unknown variables of δ_x and δ_{dc} defined as follows:

$$\frac{di_x}{dt} = -k_1 i_x + k_2(u_x - v_x) + \delta_x \quad | x = \{a, b\} \tag{10}$$

$$\frac{dv_{dc}}{dt} = k_3 \sum_{x=\{a,b,c\}} i_x s_x + \delta_{dc} \tag{11}$$

where $k_1 = R_0/L_0$, $k_2 = 1/L_0$, and $k_3 = 1/C_0$ are known parameters calculated from nominal values (R_0, L_0, and C_0). Note that the converter's terminal voltages are directly determined by switching states as follows [3], [9]:

$$\begin{bmatrix} v_a \\ v_b \\ v_c \end{bmatrix} = \frac{v_{dc}}{3} \begin{bmatrix} 2 & -1 & -1 \\ -1 & 2 & -1 \\ -1 & -1 & 2 \end{bmatrix} \begin{bmatrix} s_a \\ s_b \\ s_c \end{bmatrix} \tag{12}$$

Then, the robustness of model (10–11) depends on the successful estimation of added variables δ_x and δ_{dc}. In this paper, v_{dc}, u_x, and i_x are measured and feedbacked to the control

system, v_x are also available from the switching state from (12). Hence, the observers are designed as:

$$\dot{\hat{i}}_x = -k_1\hat{i}_x + m_2(u_x - v_x) + \hat{\delta}_x + \frac{i_x - \hat{i}_x}{\varepsilon},\ \dot{\hat{\delta}}_x = \frac{i_x - \hat{i}_x}{\varepsilon^2} \tag{13}$$

$$\dot{\hat{v}}_{dc} = k_3 \sum_{x=\{a,b,c\}} s_x i_x + \hat{\delta}_{dc} + \frac{v_{dc} - \hat{v}_{dc}}{\varepsilon},\ \dot{\hat{\delta}}_{dc} = \frac{v_{dc} - \hat{v}_{dc}}{\varepsilon^2} \tag{14}$$

To prove the convergence of (13) (i.e., $\hat{\delta}_x \to \delta_x$) as an example, the following Lyapunov function is adopted:

$$V(t) = \frac{1}{2}(i_x - \hat{i}_x)^2 + \frac{\varepsilon^2}{2}(\delta_x - \hat{\delta}_x)^2 > 0 \tag{15}$$

By substituting (10) and (13) while deriving the time-derivative of (15), the result is obtained as

$$\begin{aligned}\dot{V}(t) =& -(k_1 + \frac{1}{\varepsilon})(i_x - \hat{i}_x)^2 + \varepsilon^2(\delta_x - \hat{\delta}_x)\dot{\delta}_x \\ \leq& -(k_1 + \frac{1}{\varepsilon})(i_x - \hat{i}_x)^2 + \varepsilon^2\left|\delta_x - \hat{\delta}_x\right|\left|\dot{\delta}_x\right| \\ \leq& 0 \quad |0 < \varepsilon << 1, k_1 > 0\,. \end{aligned} \tag{16}$$

The inequality (16) is true provided that ε is small enough. This indicates the convergence of the estimated values to the true ones (i.e., $\hat{\delta}_x \to \delta_x$) with a suitable gain selection based on ε. The proof is similarly applied to (14) for the estimation of δ_c. This kind of designed observers can deal with fast-varying disturbances [3], [11], [12], [39].

Remark 1: Finite control set (FCS) model predictive control (MPC) is reported as a robust control method in the literature [9], [40], [41] due to the direct selection of discrete switching states. However, the design of a robust prediction model in this subsection is expected to further improve the robustness of the conventional FCS-MPC.

B. Fast Dynamic Control Design With Deadbeat Control Inputs

This subsection develops a deadbeat control strategy as the fastest digital control to enhance the dynamic response of the designed control system. By using (10) and (13) for model prediction of currents, a simple forward Euler's approximation is applied to (10) as

$$i_x^+ = i_x + t_s\left(-k_1 i_x + k_2 u_x - k_2 v_x + \hat{\delta}_x\right) \tag{17}$$

where the superscript ($^+$) indicates the one-step ahead prediction of the relevant variable. The variables without the superscript denote the current state of variables.

Deadbeat control inputs ($v^{db}{}_x$) are determined by simply setting the predicted values to the relevant references as in the following:

$$i_x^+ = i_x^{ref} \leftrightarrow v_x^{db} = u_x + \frac{\hat{\delta}_x - k_1 i_x}{k_2} - \frac{i_x^{ref} - i_x}{k_2 t_s} \tag{18}$$

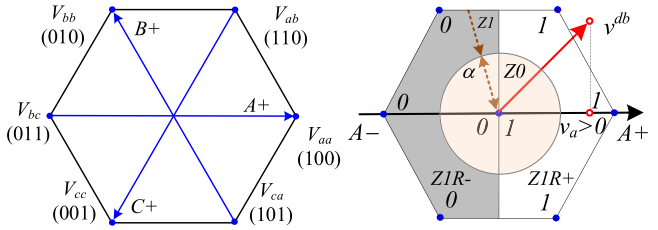

Fig. 2. Simple algorithm to directly select switching states based on continuous deadbeat control inputs in *abc*-frame, switching space of all possible vectors (left) and sub-regions to determine switching state of one individual leg (e.g., phase *a*) (right).

where $i_{abc}^{ref} = T_{dq\to abc} i_{dq}^{ref}$,

$$T_{dq\to abc} = \sqrt{\frac{2}{3}}\begin{bmatrix} \cos(\omega t) & \cos(\omega t - \frac{2\pi}{3}) & \cos(\omega t + \frac{2\pi}{3}) \\ -\sin(\omega t) & -\sin(\omega t - \frac{2\pi}{3}) & -\sin(\omega t + \frac{2\pi}{3}) \end{bmatrix}^T,$$

and $i_{dq}^{ref} = i_{dq}^{(1)ref} + \sum_{n\neq 1} i_{dq}^{(n)ref}$ as shown in (5) and (7). For charging station applications, $\overline{P}_{ref}$ in (7) is determined by an outer control loop to stabilize the *dc*-voltage (v_{dc}) at a reference value $v^{ref}{}_{dc}$. An observer-based feedforward PI control is designed for v_{dc} regulation as follows:

$$i_c^{ref} = k_p e_{dc} + k_i \int e_{dc} dt,\ i_{dc}^{ref} = i_c^{ref} - \hat{\delta}_{dc},\ \bar{P}_{ref} = v_{dc} i_{dc}^{ref} \tag{19}$$

where $e_{dc} = v_{dc} - v_{dc}^{ref}$, k_p and k_i are proportional and integral coefficients of the PI control. i_c and i_{dc} are the current through capacitor and total *dc*-current from the converter, respectively, as shown in Fig. 1(b). By substituting (19) into (11), it is easy to prove the stability of the closed-loop dynamics for the *dc*-voltage regulation under the designed PI controller.

It is noted that all calculations are conducted in the *abc*-frame for two-phases only (e.g., phases *a* and *b*) because the three-wire system satisfies the following conditions:

$$\sum_{x=\{a,b,c\}} u_x = 0;\ \sum_{x=\{a,b,c\}} i_x = 0;\ \sum_{x=\{a,b,c\}} v_x = 0 \tag{20}$$

C. Simple Algorithm to Directly Select Switching States Without Exhaustive Search

This subsection proposes a simple algorithm to directly select the switching states from the deadbeat control inputs in the *abc*-frame. As illustrated in Fig. 2, the switching state of one phase (e.g., phase *a*) is determined via the location of the deadbeat input vector (v^{db}) belonging to one of three sub-zones/regions, namely (*Z0*, *Z1R*–, and *Z1R*+). In zone *Z0*, v^{db} is small and the zero-vector is the nearest vector, hence the switching state (0, 0, 0) or (1, 1, 1), is assigned. In this case, s_x can be 0 or 1 to minimize the average switching frequency. In zone 1 (*Z1*), sub-region (*R*–), namely *Z1R*–, where $v_a < 0$, an active vector is selected and "0" switching state is assigned to s_a. Similarly, the switching state "1" is assigned to s_a with respect to *Z1R*+ for $v_a \geq 0$.

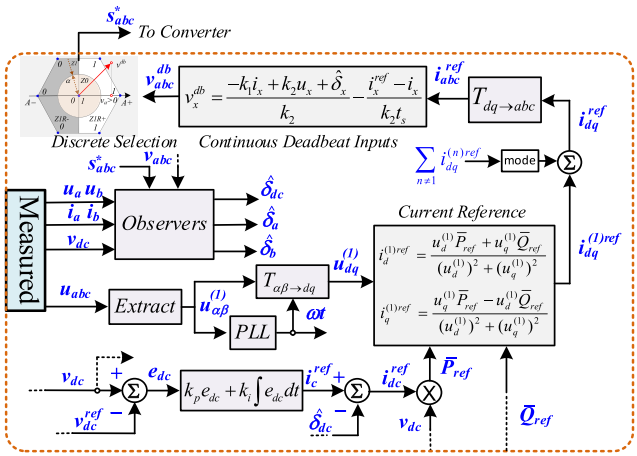

Fig. 3. Block diagram of the proposed control structure to enhance the performance and support from charging stations under critical distorted grid conditions by cancelling out all harmonic and negative current components.

The algorithm is then simply programed as (21) for 6 active vectors and (22) for 2 zero-vectors.

$$s^*_{abc} = [(v^{db}_a > 0); (v^{db}_b > 0); (v^{db}_c > 0)]$$
$$\text{where } (v^{db}_x > 0) = \{0; 1\}\ w.r.t\ \{\text{true; false}\} \tag{21}$$

$$\begin{cases} s^*_{abc} = [0;0;0] \text{ if } \left|V^{db}_i\right| < \alpha \cap SumBit\,[S^*_{abc}(k-1)] < 2 \\ s^*_{abc} = [1;1;1] \text{ if } \left|V^{db}_i\right| < \alpha \cap SumBit\,[S^*_{abc}(k-1)] \geq 2 \end{cases} \tag{22}$$

Note that the proposed algorithm can efficiently select the active vector nearest to the deadbeat vector to maximize the control performance as the deadbeat control is well known as the fastest digital control method [11]. Furthermore, this algorithm can reduce the switching frequency by selecting the optimal switching state in *Z0* compared to the previous switching state. This algorithm can avoid the exhaustive search involved in the conventional FCS-MPC, reduce the associated computational burden, and improve the overall control performance. Therefore, the proposed control system can be considered as a special version of the FCS-MPC without using any modulation stage where the robustness and simplicity of the FCS-MPC are enhanced. Extension of this algorithm for NPC or MMC topologies in high-power applications is possible with a little modification in the switching-state selection. For the multilevel converters, there are more options of switching states for one control input vector. Therefore, the proposed algorithm will have more chances to minimize the switching frequency.

The proposed control structure is detailed in Fig. 3 where the "Extract" block has a function to extract the positive sequency fundamental component of grid-voltages by adopting the common delayed-signal-cancellation (DSC) technique. It is worth noting that there is a delay time only at the beginning of the extraction process. After that, the distorted components will be detected fast provided that the positive-sequence fundamental component is relatively stable. Hence, the extraction process will affect the overall response of the designed control system at the initial instant of fundamental component detection. In practice, the fundamental component is stably regulated by the utility. Meanwhile, other distorted components can occur suddenly and unexpectedly. These conditions will not affect the overall dynamic response of the designed control system. However, in case that there are some sudden changes in the fundamental components and there is a requirement on a fast dynamic response for that change, the delay of extraction process at the beginning of the fundamental component change should be improved. The "mode" block represents options to switch between the normal operation mode and the compensating mode of the charging station. The normal mode, the dc-bus voltage, sinusoidal converter's current waveforms, and high power-factor are the control targets for converter control. In this mode, all the unbalanced harmonic current components are rejected despite the distortion in the grid voltages. In compensating mode, the unbalanced harmonic components from local nonlinear loads are additionally set as references to be compensated.

Theoretically, the proposed control structure offers following advantages compared to other control schemes in the literature. First, all the controllers are designed and implemented in an *abc*- natural frame. Hence, the control structure is much simpler by avoiding any intermediate transformation into the *dq*-frame. Second, the sequence and harmonic component extraction is only required for the fundamental positive grid voltage (u_{abc}→$u^{(1)}{}_{dq}$) for the whole control system. Meanwhile, most of the conventional methods need to extract other sequence/harmonic components of not only voltages but also currents. Third, the proposed control structure uses only one composite current controller for two-phases because the current references are summed up before entering the current controller thanks to the predictive control methodology. Meanwhile, conventional control structures are divided into multiple current-controllers for negative/high-harmonic current component control, making a complicated structure [42]. Fourth, the direct selection of switching states without exhaustive search based on simple predictive deadbeat inputs avoids computational burdens from the conventional exhaustive search in the FCS-MPC. The switching frequency is also minimized without forfeiting control performances using a very simple approach by selecting zero switching-states in Zone 0 (*Z0*) as presented in Fig. 2 (i.e., this approach is more efficient in multi-level converter topologies). Fifth, the proposed single control structure can manage and conduct multiple control tasks including regulating fundamental current components and cancelling out other unexpected components. Consequently, the instantaneous real power can be stabilized with less ripples on v_{dc}. In addition, the reactive power can be controlled to improve the power factor of the local loads. The grid-support mode can be applied for charging stations with the proposed control strategy. That is, a single-phase grid-fault is considered in the operation of the converter and the charging station is expected to maintain proper operation under the fault. In addition, the power quality of the connected distribution network can be supported by compensating the harmonic currents as well as the reactive power. In essence, the charging station can support local loads where the currents injected from the charging station to the connected grid are compensated for the reactive power and unbalanced distorted components. All these functions will be investigated in Section IV.

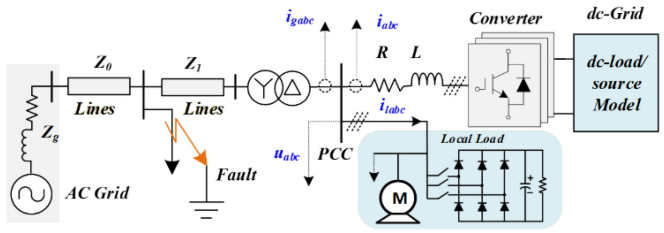

(a)

(b)

Fig. 4. Set-up for comparative studies, (a) Schematic diagram of the investigated system, (b) Photography of OPAL-RT based real-time system for performance verification.

IV. Comparative Studies and Performance Verification

This section presents comparative studies among the conventional PI controller (*PI*), the FCS-MPC structure (*FCS-MPC*), and the proposed control structure (*PRO*) under critical cases including unbalanced grid fault and harmonic distorted grid-voltage, low power-factor, unbalanced and harmonic distorted local loads. Note that single-phase to ground grid-faults are considered as a critical case of unbalanced condition which is selected for investigation in this section. The Matlab/Simulink and real-time OPAL-RT based systems are used to conduct studies and verify the comparative performances, respectively.

A. Test System for Comparative Studies

Fig. 4 illustrates the investigation set-up under comparative studies. A 60 [kW] charging-station connected to a 22 [kV] radial distribution system via a Y/Δ transformer at the PCC is shown in Fig. 4. The local loads including low power-factor, unbalanced and harmonic distorted ones connected to the PCC are shown in Fig. 4(a). In Fig. 4(b), the real-time OPAL-RT based system used for comparative performance verification is photographed. Table I lists the main parameters of the investigation set-up. For a fair comparison, three control structures are implemented with the same sampling frequency, at 25[kHz], equivalent switching frequency ($\leq$ 5[kHz]), same system settings and scenarios. For the robustness of the predictive methods, $\pm$50% uncertainty is applied to values of parameters (R, L, C).

B. Performance Under Unbalanced Grid Conditions

Fig. 5 shows comparative performances of the three investigated control structures (i.e., *PI*, *FCS-MPC*, and *PRO*) for the charging station obtained from Matlab/Simulink platforms while Fig. 6 presents the performance verification of *FCS-MPC* and *PRO* using RT-lab OPAL-RT system. The main measured indices are tabulated in Table II.

The grid is suddenly changed into a critical unbalanced condition at t = 2 [s] shown in Fig. 5 by a single phase-to-ground fault (i.e., phase b to ground fault) as indicated in Fig. 4(a). This fault causes a critical unbalanced grid voltage in the grid at the PCC with a negative voltage sequence accounting for 37% of the fundamental one. As seen in Figs. 5 and 6, all the control structures show good control performances at the balanced grid conditions (t $<$ 2 [s]), good v_{dc} regulation (i.e., almost zero steady-state error (SSE) and no ripples), and sinusoidal current waveforms with a total harmonic distortion (THD) of around 2% as listed in Table II.

However, at critical unbalanced conditions, *PI* shows a significant steady-state error, i.e., SSE(v_{dc}) = 27.2[V], and highly unbalanced and distorted grid currents (36.5[A] for negative peak current and 8.08% for maximum THD in phase b. Meanwhile, the *FCS-MPC* and the *PRO* show better performances

TABLE I
Main Parameters the Investigated Distribution Network

System rate power of AC Grid	S_n	10 [MVA]
MV rated voltage	U_M	22 [kV]
LV rated line-to-line voltage	U_L	400 [V]
Filter resistance	R	1 [Ω]
Filter reactance	L	10 [mH]
Nonlinear rectifier load	R_L, C_L	40 [Ω], 400 [μF]
Rated power, power factor of motor	P	10 [kW], 0.7
Rated *dc*-voltage	V_{dc}	600[V]
dc-link capacitance	C	4.7 [mF]
Switching frequency	f_z	5 [kHz] for PI ($<$ 5 kHz) for others
Sampling frequency	f_s	25 [kHz]

TABLE II
Comparative Performance Indices of Investigated Control Structures

Indices [unit]	*PI*	*FCS-MPC*	*PRO*
Balanced Grid Voltage			
SSE/Ripple(v_{dc}) [V]	0/$\pm$0.1	0/$\pm$0.1	0/$\pm$0.1
$I^{(n)}{}_{Peak}$ (b) [A]	0.35	0.45	0.25
THD (a,b,c) [%]	(2.69, 2.74, 2.65)	(2.11, 2.00, 2.10)	(1.94, 1.90, 1.97)
Critical Unbalanced Grid Voltage			
SSE/Ripple(v_{dc}) [V]	27.2/$\pm$9.0	0/$\pm$9.5	0/$\pm$7.5
$I^{(-1)}{}_{Peak}$ (b) [A]	36.5	7.4	4.5
THD (a,b,c) [%]	(4.78, 8.08, 2.39)	(2.45, 4.62, 3.19)	(3.3, 3.36, 1.29)
Unbalanced and Distorted Grid Voltage			
SSE/Ripple(v_{dc}) [V]	0.1/$\pm$4.6	0/$\pm$8.5	0/$\pm$5.3
$I^{(n)}{}_{Peak}$ (b) [A]	28.5	5.5	3.0
THD (a,b,c) [%]	(13.9, 15.3, 14.9)	(4.92, 5.50, 4.10)	(4.57, 4.68, 3.55)
Local Load Support Mode for PRO Only			
SSE/Ripple(v_{dc}) [V]	0/$\pm$0.5		
$I^{(n)}{}_{Peak}$ (b) [A]	3.1		
THD(a,b,c) [%] i_{load}/i_{grid}	(11.64,11.64, 11.64)/(3.12, 3.29, 2.25)		

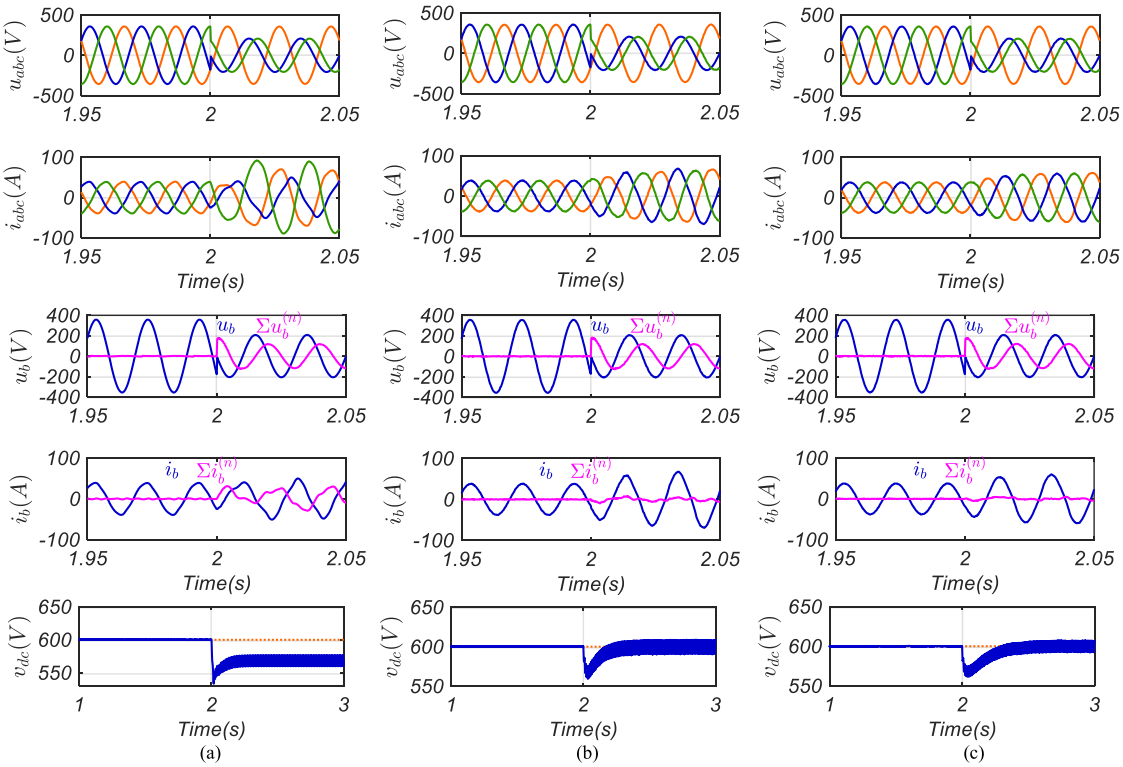

Fig. 5. Comparative performance under unbalanced condition in grid fault obtained from Matlab/Simulink platforms, (a) The conventional PI control structure (*PI*), (b) The FCS-MPC structure (*FCS-MPC*), (c) The proposed control structure (*PRO*).

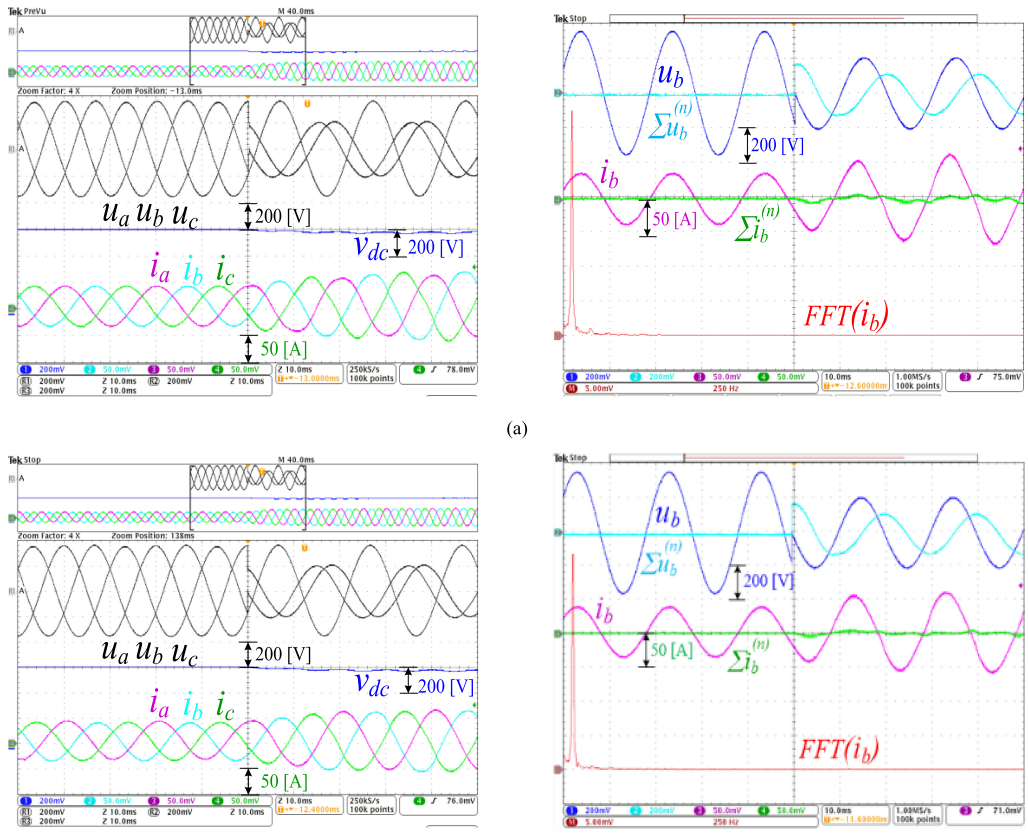

Fig. 6. Performance verification on RT-Lab OPAL-RT System, (a) The FCS-MPC structure (*FCS-MPC*), (b) The proposed control structure (*PRO*).

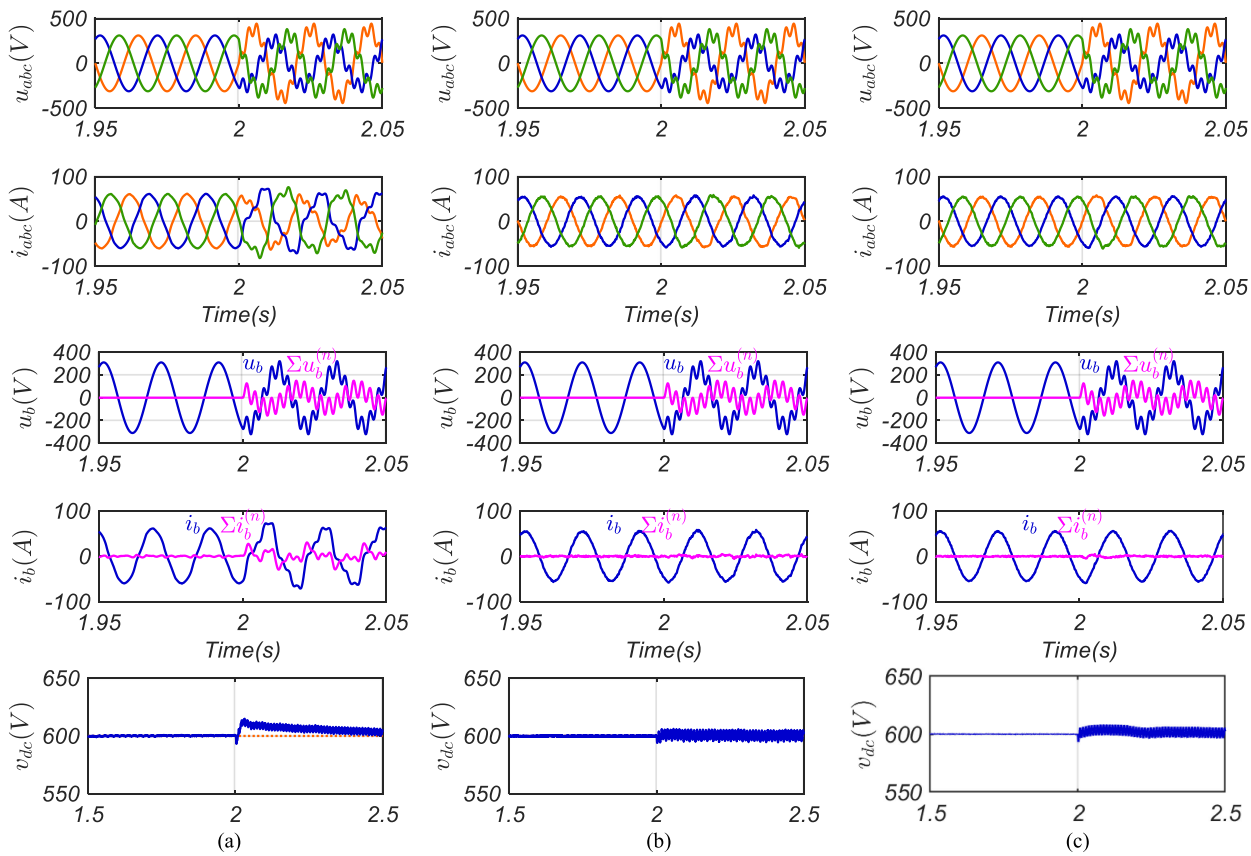

Fig. 7. Comparative performance under general harmonic voltage conditions obtained from Matlab/Simulink platform, (a) The conventional PI control structure, (b) The FCS-MPC structure, (c) The proposed control structure.

in terms of the v_{dc} dynamic response and current regulation as seen from the comparative v_{dc} and total undesired current component $\Sigma i^{(n)}{}_b$ ($n \neq 1$) waveforms in Figs. 5 and 6. With a special control structure, the proposed method offers the best dynamic response and regulation on v_{dc}, best current balance and sinusoidal waveforms among the investigated structures as seen in subfigures on the right-side of Figs. 5 and 6. The better performance of the proposed control structure can be explained by a fast-dynamic response of direct predictive control methods and the ability to cancel out general harmonics.

C. Performance Under General Distorted Grid Voltages

This section investigates a more critical condition under both unbalanced and general harmonic distorted grid voltages as shown in Fig. 7 (i.e., obtained from Matlab/Simulink platforms) where from t = 2[s], an unbalance of 25% and 7$^{\text{th}}$ harmonic component of 25% are imposed to the balanced grid voltages. Note that the unrealistic distortion of voltages used for investigation (25%) to show the limits of voltage distortion that the proposed control system can maintain their currents injected into the grid (i.e., around 5% of THD). Fig. 8 shows the verification results from the *FCS-MPC* and the *PRO* on the real-time system.

As shown in Fig. 7(a), the *PI* can work well in the balanced grid voltage by an acceptable v_{dc} and grid current regulation as shown in the previous subsection. However, unacceptable performances on the grid current regulation are seen in the critical case of both unbalanced and harmonic distorted voltages (i.e., 28.5[A] for negative-sequence peak current, maximum harmonic of 15.3% in phase *b*). The better performances of the *FCS-MPC* are seen from Fig. 7(b) and Fig. 8(a) because of faster dynamic current response. However, the best improvements are shown in Fig. 7(c) and Fig. 8(b) with the *PRO* where both v_{dc} and the total current harmonic components are regulated at low errors. The v_{dc} ripples of the *PRO* are smaller in amplitude and with less harmonic components than the ones of *FCS-MPC*. Especially, significant fast dynamics are observed from direct predictive methods (*FCS-MPC* and *PRO*.) in comparison with the PI method. The comparative measured indices are shown in Table II for easy comparison. In Fig. 8, the proposed structure exhibits better control performances where the current harmonic spectrums of i_b are shown. The purpose to show the Fast-Fourier-Transform (FFT) of phase-*b* converter current (i_b) is to qualitatively compare the current control quality among controllers. That is, the FFT exhibits the fundamental and harmonic components in magnitudes for easy comparison. The THDs are measured and listed in Table II for an easy comparison among the three methods.

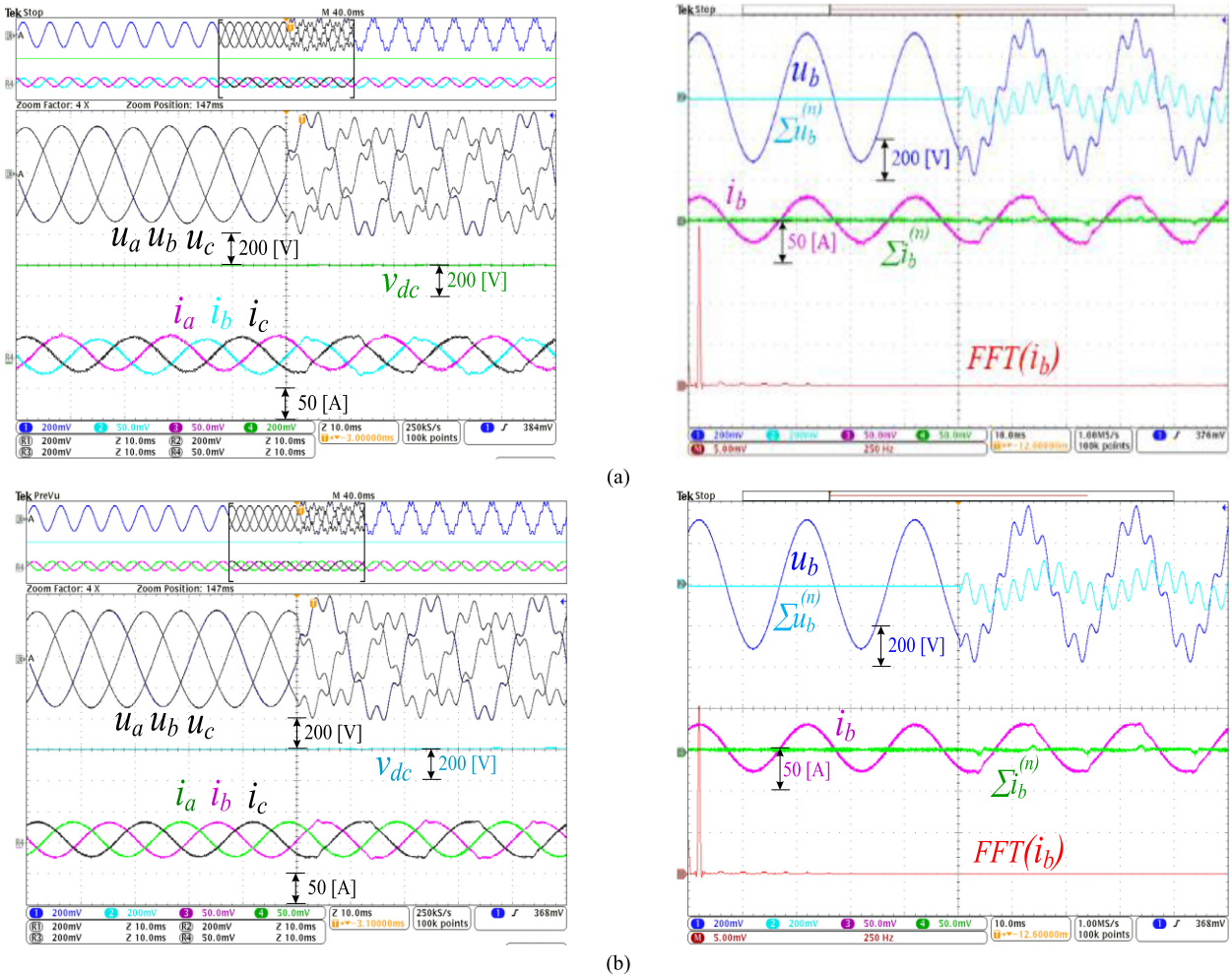

Fig. 8. Comparative verification on RT-Lab OPAL RT System, (a) The FCS-MPC structure, (b) The proposed control structure.

D. Reactive Power and Unbalanced Harmonic Current Compensation for Local Loads

This subsection proposes a special operation mode of the charging station where it maintains the power supply to charging loads and at the same time, supports the local loads. There are two kinds of support offered by controlling the interface converter of the charging station: reactive power compensation and unbalanced harmonic current compensation for the local loads. This kind of support from the charging station can help to improve the power-quality of the grid. This mode is realized by the proposed method thanks to the special design of the proposed structure (*PRO*).

The scenario is shown in Fig. 9 with "OFF" mode before the triggering time (the center of scope) and "ON" mode after that. The 10 kW three-phase local load is made unbalanced by connecting only two among three phases (phase *a* opened) where the harmonic currents are generated by three-phase diode-based rectifier as shown in Fig. 4(a). In the "OFF" mode, the PRO shows good regulations on v_{dc} and converter currents i_{abc} as seen in Fig. 9. However, the local load consumes 10 [kVAr] reactive power making the local load currents, i_{lb} lagging the PCC voltage, u_b as seen with the phase *b* in Fig. 9(b) before the triggering instant in the "OFF" mode. In addition, a high distortion can be observed from a current of the three-phase diode-rectifier, i_{lb}, making the THD of local load currents at 11.64%. Hence, the grid currents i_{gabc} are unbalanced and distorted by the local loads in the "OFF" mode. After the triggering instant, in the "ON" mode, the inverter currents are both shifted and distorted to compensate for the local loads as seen in Fig. 9 on the right-side of each subfigure.

Consequently, converter currents are shifted to lead the voltage, and additional harmonics are generated as seen in Fig. 9(b), in the "ON" mode. The charging station converter generates a leading current, i_b with opposite current harmonics to compensate both the unbalanced and harmonic current from the local loads. Consequently, in the "ON" mode, i_{gb} is in phase with u_b for unity power factor at the PCC, and the grid current harmonics are significantly removed to make the THD reduced to about 3.29% as shown in Table II.

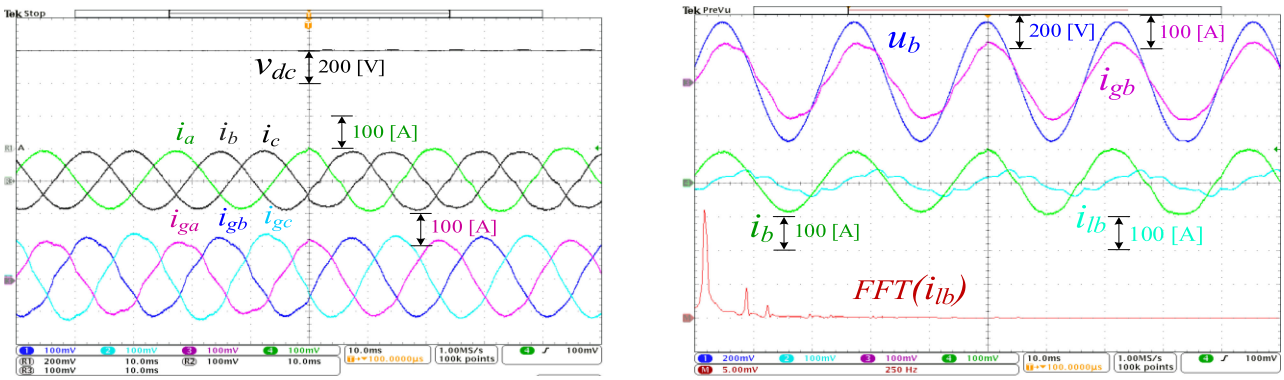

Fig. 9. Performance verification in local load support mode with both reactive and harmonic current compensation. (a) Voltage and current performance. (b) Phase shift and harmonic generation for compensation.

V. Conclusion

This paper proposed a new control structure accompanied by an effective direct predictive control algorithm to enhance performance and support from charging stations under critical conditions of grids. The grid-interfaced converters are controlled to cancel out the undesired harmonic current components while maintaining a stable *dc*-link voltage. Comparative studies on Matlab/Simulink and verification on OPAL-RT based systems show significant improvements under critical grid conditions in terms of fast dynamic response and precise control of *dc*-link voltage, balanced sinusoidal grid currents under both transient and steady states. Especially, a special grid-support mode for critical local loads is proposed to effectively compensate for reactive power, unbalanced and distorted load currents. Based on this performance, the proposed control structure can be extended to high-power applications with multilevel converters (e.g., NPC and MMC). The strategy can be also extensively applied into various power electronics systems such as adjustable speed drives, motor drives, renewable energy sources, energy storage systems, and active filters.

References

[1] S. S. Williamson, A. K. Rathore, and F. Musavi, "Industrial electronics for electric transportation: Current state-of-the-art and future challenges," *IEEE Trans. Ind. Electron.*, vol. 62, no. 5, pp. 3021–3032, May 2015.

[2] T. Qian, C. Shao, X. Li, X. Wang, and M. Shahidehpour, "Enhanced coordinated operations of electric power and transportation networks via EV charging services," *IEEE Trans. Smart Grid*, vol. 11, no. 4, pp. 3019–3030, Jul. 2020.

[3] H. T. Nguyen and J. W. Jung, "Asymptotic stability constraints for direct horizon-one model predictive control of SPMSM drives," *IEEE Trans. Power Electron.*, vol. 33, no. 10, pp. 8213–8219, Oct. 2018.

[4] H. T. Nguyen *et al.*, "Further optimized scheduling of micro grids via dispatching virtual electricity storage offered by deferrable power-driven demands," *IEEE Trans. Power Syst.*, vol. 35, no. 5, pp. 3494–3505, Sep. 2020.

[5] K. W. Hu and C. M. Liaw, "Incorporated operation control of DC microgrid and electric vehicle," *IEEE Trans. Ind. Electron.*, vol. 63, no. 1, pp. 202–215, Jan. 2016.

[6] International Renewable Energy Agency (IRENA) Abu Dhabi, "Innovation landscape brief: Electric-vehicle smart charging," 2019. [Online]. Available: www.irena.org/publications

[7] F. Mwasilu, J. J. Justo, E. K. Kim, T. D. Do, and J. W. Jung, "Electric vehicles and smart grid interaction: A review on vehicle to grid and renewable energy sources integration," *Renewable Sustain. Energy Rev.*, vol. 34, pp. 501–516, 2014.

[8] S. J. Wu, H. T. Nguyen, and W. C. Chien, "Optimal cooperative demand response scenario for system congestion," *Int. J. Power Energy Syst.*, vol. 35, no. 3, pp. 85–94, 2015.

[9] H. T. Nguyen, J. Kim, and J. W. Jung, "Improved model predictive control by robust prediction and stability-constrained finite states for three-phase inverters with an output LC filter," *IEEE Access*, vol. 7, pp. 12673–12685, 2019.

[10] H. Nguyen, A. S. Al-Sumaiti, K. Turitsyn, Q. Li, and M. S. El Moursi, "Further optimized scheduling of micro grids via dispatching virtual electricity storage offered by deferrable power-driven demands," *IEEE Trans. Power Syst.*, vol. 35, no. 5, pp. 3494–3505, Sep. 2020.

[11] H. T. Nguyen and J. W. Jung, "Disturbance-rejection-based model predictive control: Flexible-mode design with a modulator for three-phase inverters," *IEEE Trans. Ind. Electron.*, vol. 65, no. 4, pp. 2893–2903, Mar. 2018.

[12] H. T. Nguyen, E. K. Kim, I. P. Kim, H. H. Choi, and J. W. Jung, "Model predictive control with modulated optimal vector for a three-phase inverter with an LC filter," *IEEE Trans. Power Electron.*, vol. 33, no. 3, pp. 2690–2703, Mar. 2018.

[13] P. T. Staats, W. M. Grady, A. Arapostathis, and R. S. Thallam, "A statistical analysis of the effect of electric vehicle battery charging on distribution system harmonic voltages," *IEEE Trans. Power Del.*, vol. 13, no. 2, pp. 640–646, Apr. 1998.

[14] S. Martinenas, K. Knezovic, and M. Marinelli, "Management of power-quality issues in low voltage networks using electric vehicles: Experimental validation," *IEEE Trans. Power Del.*, vol. 32, no. 2, pp. 971–979, Apr. 2017.

[15] M. Singh, V. Khadkikar, A. Chandra, and R. K. Varma, "Grid interconnection of renewable energy sources at the distribution level with power-quality improvement features," *IEEE Trans. Power Del.*, vol. 26, no. 1, pp. 307–315, Jan. 2011.

[16] A. Kirakosyan, M. S. El Moursi, and V. Khadkikar, "Fault ride through and grid support topology for the VSC-HVDC connected offshore wind farms," *IEEE Trans. Power Del.*, vol. 32, no. 3, pp. 1592–1604, Jun. 2017.

[17] J. Jia, G. Yang, and A. H. Nielsen, "A review on grid-connected converter control for short-circuit power provision under grid unbalanced faults," *IEEE Trans. Power Del.*, vol. 33, no. 2, pp. 649–661, Apr. 2018.

[18] M. M. Shabestary and Y. A. R. I. Mohamed, "Advanced voltage support and active power flow control in grid-connected converters under unbalanced conditions," *IEEE Trans. Power Electron.*, vol. 33, no. 2, pp. 1855–1864, Feb. 2018.

[19] Y. Zhang, J. Jiao, and J. Liu, "Direct power control of PWM rectifiers with online inductance identification under unbalanced and distorted network conditions," *IEEE Trans. Power Electron.*, vol. 34, no. 12, pp. 12524–12537, Dec. 2019.

[20] A. Kumar and G. Srungavarapu, "Algorithm-based direct power control of active front-end rectifiers," *IET Power Electron.*, vol. 12, no. 4, pp. 712–718, 2019.
[21] M. Pahlevaninezhad, P. Das, J. Drobnik, P. K. Jain, and A. Bakhshai, "A new control approach based on the differential flatness theory for an AC/DC converter used in electric vehicles," *IEEE Trans. Power Electron.*, vol. 27, no. 4, pp. 2085–2103, Apr. 2012.
[22] D. C. Lee, G. M. Lee, and K. D. Lee, "DC-bus voltage control of three-phase AC/DC PWM converters using feedback linearization," *IEEE Trans. Ind. Appl.*, vol. 36, no. 3, pp. 826–833, May/Jun. 2000.
[23] Y. Shtessel, S. Baev, and H. Biglari, "Unity power factor control in three-phase AC/DC boost converter using sliding modes," *IEEE Trans. Ind. Electron.*, vol. 55, no. 11, pp. 3874–3882, Nov. 2008.
[24] J. Fernando Silva, "Sliding-mode control of boost-type unity-power-factor PWM rectifiers," *IEEE Trans. Ind. Electron.*, vol. 46, no. 3, pp. 594–603, Jun. 1999.
[25] H. Fehr and A. Gensior, "On trajectory planning, backstepping controller design and sliding modes in active front-ends," *IEEE Trans. Power Electron.*, vol. 31, no. 8, pp. 6044–6056, Aug. 2016.
[26] J. Liu, S. Laghrouche, and M. Wack, "Observer-based higher order sliding mode control of power factor in three-phase AC/DC converter for hybrid electric vehicle applications," *Int. J. Control*, vol. 87, no. 6, pp. 1117–1130, 2014.
[27] T. Noguchi, H. Tomiki, S. Kondo, and I. Takahashi, "Direct power control of PWM converter without power-source voltage sensors," *IEEE Trans. Ind. Appl.*, vol. 34, no. 3, pp. 473–479, May/Jun. 1998.
[28] D. Zhi, L. Xu, and B. W. Williams, "Improved direct power control of grid-connected DC / AC converters," *IEEE Trans. Power Electron.*, vol. 24, no. 5, pp. 1280–1292, May 2009.
[29] A. Yazdani and R. Iravani, "A unified dynamic model and control for the voltage-sourced converter under unbalanced grid conditions," *IEEE Trans.Power Delivery*, vol. 21, no. 3, pp. 1620–1629, Jul. 2006.
[30] Y. Zhang, C. Qu, and S. Member, "Table-Based direct power control for three-phase AC/DC converters under unbalanced grid voltages," *IEEE Trans. Power Electron.*, vol. 30, no. 12, pp. 7090–7099, Dec. 2015.
[31] Y. Zhang, C. Qu, and J. Gao, "Performance improvement of direct power control of PWM rectifier under unbalanced network," *IEEE Trans. Power Electron.*, vol. 32, no. 3, pp. 2319–2328, Mar. 2017.
[32] H. Nian, S. Member, Y. Shen, H. Yang, and Y. Quan, "Flexible grid connection technique of voltage-source inverter under unbalanced grid conditions based on direct power control," *IEEE Trans. Ind. Appl.*, vol. 51, no. 5, pp. 4041–4050, Sep./Oct. 2015.
[33] P. Cheng and H. Nian, "Direct power control of voltage source inverter in a virtual synchronous reference frame during frequency variation and network unbalance," *IET Power Electron.*, vol. 9, no. 3, pp. 502–511, 2016.
[34] X. Guo, Y. Yang, and X. Zhang, "Advanced control of grid-connected current source converter under unbalanced grid voltage conditions," *IEEE Trans. Ind. Electron.*, vol. 65, no. 12, pp. 9225–9233, Dec. 2018.
[35] F. Nejabatkhah, Y. Li, and B. Wu, "Control strategies of three-phase distributed generation inverters for grid unbalanced voltage compensation," *IEEE Energy Convers. Congr. Expo. ECCE 2015*, vol. 31, no. 7, pp. 6467–6474, 2015.
[36] Y. Zhang, Z. Wang, J. Jiao, and J. Liu, "Grid-Voltage sensorless model predictive control of three-phase PWM rectifier under unbalanced and distorted grid voltages," *IEEE Trans. Power Electron.*, vol. 35, no. 8, pp. 8663–8672, Aug. 2020.
[37] X. H. Wu, S. K. Panda, and J. X. Xu, "DC link voltage and supply-side current harmonics minimization of three phase PWM boost rectifiers using frequency domain based repetitive current controllers," *IEEE Trans. Power Electron.*, vol. 23, no. 4, pp. 1987–1997, Jul. 2008.
[38] K. Ma, "Limits of the power controllability of three-phase converter with unbalanced AC source," *Res. Top. Wind Energy*, vol. 5, pp. 189–196, 2015.
[39] T. D. Do and H. T. Nguyen, "A generalized observer for estimating fast-varying disturbances," *IEEE Access*, vol. 6, pp. 28054–28063, 2018.
[40] H. T. Nguyen and J. W. Jung, "Finite control set model predictive control to guarantee stability and robustness for surface-mounted PM synchronous motors," *IEEE Trans. Ind. Electron.*, vol. 65, no. 11, pp. 8510–8519, Nov. 2018.
[41] F. Mwasilu, H. T. Nguyen, H. H. Choi, and J. W. Jung, "Finite set model predictive control of interior PM synchronous motor drives with an external disturbance rejection technique," *IEEE/ASME Trans. Mechatronics*, vol. 22, no. 2, pp. 762–773, Apr. 2017.
[42] A. Moawwad, M. S. El Moursi, and W. Xiao, "A novel transient control strategy for VSC-HVDC connecting offshore wind power plant," *IEEE Trans. Sustain. Energy*, vol. 5, no. 4, pp. 1056–1069, Oct. 2014.

Hoach The Nguyen (Member, IEEE) received the B.S. degree in electrical engineering from the Hanoi University of Science and Technology, Hanoi, Vietnam, in 2007, the M.S. degree in electrical engineering from the Dayeh University, Changhua, Taiwan, in 2010, and the Ph.D. degree from the Division of Electronics and Electrical Engineering, Dongguk University, Seoul, South Korea, in 2018. In 2011, he was a Teaching Assistant with Hanoi Architectural University, Hanoi, Vietnam, and is currently on leave. Since 2018, he has been a Research Fellow with Electrical Engineering and Computer Science Department, Khalifa University, Abu Dhabi, UAE. His research interests include electric power systems, control of power converters, electric machine drives, wind turbine control, water-energy nexus, water and energy demand response, nano- and microgrids, wireless power transfer, and charging technologies for electric vehicles.

Ameena Saad Al Sumaiti (Senior Member, IEEE) received the B.Sc. degree in electrical engineering from United Arab Emirates University, UAE, in 2008, and the M.Sc. and Ph.D. degrees in electrical and computer engineering from the University of Waterloo, Waterloo, ON, Canada, in 2010 and 2015, respectively. She was a Visiting Assistant Professor with MIT, Cambridge, MA, USA, in 2017. She is currently an Assistant Professor with the Advanced Power and Energy Center and the Department of Electrical Engineering and Computer Science, Khalifa University, Abu Dhabi, United Arab Emirates. Her research interests include power systems, intelligent systems, energy economics, and energy policy.

Khalifa Al Hosani (Senior Member, IEEE) received the B.Sc. and M.Sc. degrees in electrical engineering from the University of Notre Dame, Notre Dame, IN, USA, in 2005 and 2007, respectively, and the Ph.D. degree in electrical and computer engineering from The Ohio State University, Columbus, OH, USA, in 2011. He is currently an Associate Professor with the Department of Electrical and Computer Engineering, Khalifa University, Abu Dhabi, United Arab Emirates. He is the Co-Founder of the Power Electronics and Advanced Sustainable Energy Center Laboratory, ADNOC Research and Innovation Center, Abu Dhabi, United Arab Emirates. His research interests include nonlinear control, sliding mode control, control of power electronics, power systems stability and control, renewable energy systems modeling and control, smart grid, microgrid and distributed generation, and application of control theory to oil and gas applications.

Khaled Al Jaafari (Member, IEEE) was born in Al Ain, UAE. He received the B.S. and M.S. degrees in electrical engineering from Petroleum Institute, Abu Dhabi, UAE, in 2006 and 2011, respectively, and the Ph.D. degree in electrical engineering from Texas A&M University, College Station, TX, USA, in 2016.

He is currently working with Khalifa University, Abu Dhabi, UAE, as an Assistant Professor. His research interests include machines design and condition monitoring, power system analysis, power system protection, and power quality studies.

Young-Ji Byon (Member, IEEE) was born in Seoul, South Korea, in 1979. He received the B.A.Sc. degree from the Department of Mechanical and Industrial Engineering, University of Toronto, Toronto, ON, Canada, in 2003, and the M.Sc. and Ph.D. degrees in transportation engineering from the Department of Civil and Environmental Engineering, University of Toronto, in 2005 and 2010, respectively. He moved to Toronto, ON, Canada, in 1994. From 2003 to 2009, he was a Researcher with the ITS Lab, University of Toronto. From 2009 to 2010, he was a Visiting Researcher with the University of Chile, Santiago, Chile. From 2010 to 2011, he was a Postdoctoral Research Fellow with the University of Calgary, Calgary, AB, Canada. In 2012, he joined the Department of Civil Infrastructure and Environmental Engineering, Khalifa University of Science and Technology, Abu Dhabi, United Arab Emirates, as an Assistant Professor. In 2017, he was promoted to an Associate Professor and is currently an Associate Chair of the department.

Jamal Yousuf Alsawalhi (Member, IEEE) received the B.S., M.S., and Ph.D. degrees in electrical engineering from Purdue University, West Lafayette, IN, USA, in 2009, 2011, and 2014, respectively. In 2015, he joined as a Faculty Member with Khalifa University, Abu Dhabi, United Arab Emirates, where he is currently an Assistant Professor. His research interests include electric machines and drives, wireless charging, and transportation electrification.

Mohamed Shawky El Moursi (Senior Member, IEEE) received the B.Sc. and M.Sc. degrees in electrical engineering from Mansoura University, Mansoura, Egypt, in 1997 and 2002, respectively, and the Ph.D. degree in electrical engineering from the University of New Brunswick (UNB), Fredericton, NB, Canada, in 2005. From 2002 to 2005, he was a Research and Teaching Assistant with the Department of Electrical and Computer Engineering, UNB. He joined McGill University, Montreal, QC, Canada, as a Postdoctoral Fellow with the Power Electronics Group. He joined the Wind Power Plant Group, Technology R&D, Vestas Wind Systems, Arhus, Denmark. He was with TRANSCO, UAE, as a Senior Study and Planning Engineer. He is currently a Professor with Electrical and Computer Engineering Department, Masdar Institute Research Centers, Khalifa University, Abu Dhabi, UAE, and seconded to a Professor Position with the Faculty of Engineering, Mansoura University, Mansoura, Egypt, and is currently on leave. He was a Visiting Professor with the Massachusetts Institute of Technology, Cambridge, MA, USA. His research interests include power system, power electronics, FACTS technologies, VSC-HVDC systems, microgrid operation and control, and renewable energy systems (wind and PV) integration and interconnections. He is currently the Editor of the IEEE TRANSACTIONS ON POWER DELIVERY and the IEEE TRANSACTIONS ON POWER SYSTEMS, an Associate Editor for the IEEE TRANSACTIONS ON POWER ELECTRONICS, the Guest Editor of the IEEE TRANSACTIONS ON ENERGY CONVERSION, the Guest Editor-in-Chief of special section between IEEE TRANSACTIONS ON POWER DELIVERY and IEEE TRANSACTIONS ON POWER SYSTEMS, the Editor of the IEEE POWER ENGINEERING LETTERS, the Regional Editor of the IET *Renewable Power Generation,* and an Associate Editor for the IET *Power Electronics Journals*.